PCCP

Accepted Manuscript

ROYAL SOCIETY OF CHEMISTRY

www.rsc.org/pccp

Elucidating the Enhancement in Optical Properties of Low Band Gap Polymers by Tuning the Structure of Alkyl Side Chains

Jing Lu[1], Yao Yao[2], Prathamesh M. Shenai[1], Lipeng Chen[1], and Yang Zhao[1] *
[1] *Division of Materials Science, Nanyang Technological University, 50 Nanyang Avenue, Singapore 639798*
[2] *State Key Laboratory of Surface Physics and Department of Physics, Fudan University, Shanghai 200433, China*

We carry out a computational study of optical properties of two novel 5,6-difluorobenzo[c][1,2,5]-thiadiazole-based polymers, PFBT-T20TT and PFBT-T12TT to elucidate the surprisingly superior performance of polymer solar cells based on the former, when it differs from the latter only in the alkyl side-chains. Density Functional Theory (DFT) based geometry optimization at B3LYP/6-31G(d) level reveals differences in internal coordinates, which are important in tuning the electronic and optical properties. We further calculate the electronic structure at room temperature by employing molecular dynamics (MD) simulations in combination with DFT techniques. The energies of the highest occupied molecular orbital (HOMO) are found to be in reasonable agreement with the available experimental data and the HOMO-lowest unoccupied MO energy gap is found to be similar for both the molecules. The electronic density of HOMO in PFBT-T20TT is, however, found to be significantly more delocalized along the backbone, which is proposed to be conducive to formation of charge separated states and lead to improved device performance. Furthermore, via fitting the absorption spectra calculated with the multi-mode Brownian Oscillator model, we have also extracted a weaker exciton-phonon coupling parameter in PFBT-T20TT, consistent with the trends revealed via the DFT-MD results.

I. INTRODUCTION

Polymer solar cells (PSCs) have been widely studied in the past two decades owing to their promising advantages offered in terms of low cost, versatility of functionalization, thin film flexibility, and ease of processing.[1–4] The bulk-heterojunction PSCs, in which the donor and acceptor form a blend of interpenetrating domains, exhibit a significantly improved performance compared to those based on small molecules.[5–7] Furthermore, the polymers with a relatively low band gap can more efficiently harvest solar energy and convert it to the free charge carriers. For example, with benzothiadiazole-based low band gap polymers as donor materials, the power conversion efficiency of the respective solar cells has doubled from 5% to slightly more than 10%.[8,9] The low band gap polymers are thus recognized to be the third generation semiconducting polymers, and a common design principle for their application in the PSCs involves utilization of alternating electron donor and acceptor (D-A) structure so that the energy levels of the polymers can be easily tuned.[10]

Recently, Wang *et al.* have synthesized 5,6-difluorobenzo[c][1,2,5]-thiadiazole-based D-A polymers, PFBT-T20TT and PFBT-T12TT, (see Fig. 1)[11] which exhibit potential as donor materials in low band gap PSCs.[11] The molecular structures of these two materials differ only in terms of the long alkyl chain side-groups, which are in the pendant straight and branched conformations in PFBT-T12TT and PFBT-T20TT, respectively. It was, however, found surprisingly that the devices based on the latter exhibit a remarkably superior performance. In the solar cells with polymer/$PC_{71}BM$ blend structure, the short-circuit current (I_{sc}) is greatly enhanced by nearly an order of magnitude for PFBT-T20TT as compared to PFBT-T12TT. The open-circuit voltage (V_{oc}) and the fill factors, on the other hand, were found to be nearly the same in both the devices. This effect implies that the introduction of branched chains in PFBT-T20TT exerts little influence on the band gap, evident from the nearly identical V_{oc}, but may lead to much greater mobility of electrons, causing I_{sc} to get enhanced. Organic materials under identical extrinsic conditions such as the temperature and the electric field, exhibit an enhancement in their mobility mainly due to a decrease in the degree of disorder and thereby delocalization of the electronic wave function.[12] While the branched side chains in PFBT-T20TT may influence the electronic wavefunction in an analogous manner leading to an enhancement of the mobility, the underlying physics is poorly understood. This hypothesis is corroborated by the optical experiments on thin-film PFBT-T20TT devices, which show strong broad absorption and enhanced inter-chain interactions. It thus warrants a detailed theoretical study on the inter-relationship between the molecular structures, the electronic wavefunction and the resulting device performance in these two materials in order to explain how the influence of branched alkyl chain in tuning the optical properties leads to a superior device performance in PFBT-T20TT.

Recent advances in the optical characterization techniques have helped reveal a crucial role played by the delocalization of electronic wave functions in PSCs.[13–17] There is thus a growing need, from the theoretical point of view, to be able to accurately predict the energetic structures and the optical properties of polymeric materials. In particular, how such properties are affected by molecular vibrations is a common question of consider-

*Electronic address: YZhao@ntu.edu.sg

able importance in designing and optimizing a material's performance for application in organic electronic devices. In the past decade, significant efforts with this kind of method have been devoted to the theoretical investigation of the processes of light absorption and the subsequent exciton and charge carrier transport in organic solar cells.[2,18–22] One of the most commonly used methods to characterize the ground state and excited state electronic structures in various polymeric materials involves calculations based on the Density Functional Theory (DFT). Such DFT based calculations have proved fruitful in a wide range of studies such as determination of band structure in conjugated polymers,[23] determination of crystal structure,[24] localization of electronic excitations[25] as well as orbital energy modeling.[26] Furthermore, DFT calculations have also been used in conjunction with molecular dynamics (MD) simulations, allowing one to probe the effect of temperature as well as intra- and inter-molecular vibrational modes on electronic properties of polymeric systems.[27] An alternative technique that can empirically take into account the interactions between an electronic excitation and the molecular vibrations is the multimode Brownian oscillator (MBO) model.[28–31] The MBO model describes a two-(electronic)level system coupled to a small number of primary oscillators which are, in turn, coupled linearly to a bath of secondary harmonic oscillators. This model has been successfully applied to interpret optical spectra of chromophores in liquid solutions,[32–35] as well as the absorption and emission spectra of a conjugated polymer.[36] The ever evolving spectrum of theoretical methods notwithstanding, the problem of understanding the transport properties in organic semiconductor materials still remains challenging, primarily due to the multiscale nature of the problem[37] as well as strong electron-phonon coupling.[18,38,39]

In this paper, we investigate the electronic and optical properties of PFBT-T20TT and PFBT-T12TT, aimed at explaining why the former exhibits a remarkably high performance in PSC devices than the latter. We adopt a dual-faceted approach of utilizing combined quantum chemical and MD simulations to probe the molecular properties, and using the MBO analysis to gain underlying physical insights via fitting of absorption spectra. These two complimentary approaches provide different perspective for understanding the intrinsic physics of the performance of devices based on PFBT-T20TT and PFBT-T12TT. The rest of the paper is organized as follows. The details of computational methodologies employed are provided in Section II A, whereas an overview of the MBO model is presented in Section II B. Results on optical properties calculated via quantum chemical and MD simulations along with those on MBO-derived fitting of the absorption spectra are presented and discussed in detail in Section III. Finally, we draw conclusions in Section IV.

II. THEORY AND COMPUTATIONAL DETAILS

A. Quantum Chemical Calculations and Molecular Dynamics Simulations

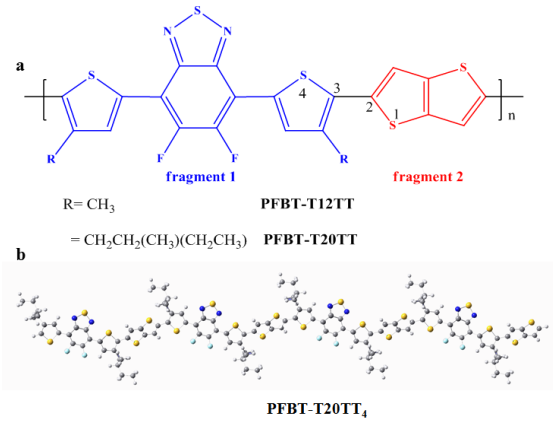

Figure 1: (a) The chemical structures of PFBT-T12TT and PFBT-T20TT as distinguished by the alkyl chain substitutions. (b) The calculated optimized geometry of PFBT-T20TT$_4$ oligomer with the number of repeat units n = 4.

We have studied the two recently synthesized novel donor-acceptor polymeric materials abbreviated as PFBT-T12TT and PFBT-T20TT.[11] The molecular structures for these two materials are presented in Fig. 1(a). The two molecules have exactly the same backbone structure but differ only in terms of the long alkyl-chain side groups (R). In PFBT-T12TT R is $C_{12}H_{25}$ group which has a long chained structure. In PFBT-T12TT, on the other hand R is a much bulkier alkyl group $CH_2CH(C_{10}H_{21})(C_8H_{17})$ which has a pendant-like branched configuration. To improve the computational efficiency in our calculations, long alkyl chains have been replaced by the methyl and methylbutyl groups in PFBT-T12TT and PFBT-T20TT, respectively, which represent smallest possible linear or branched groups. Such replacement of large side-groups with smaller analogous groups is a commonly employed approach in computational studies of polymers, as in general, their influence on the electronic and optical properties is negligible.[40] Furthermore, as the optoelectronic properties of the conjugated oligomers converge with an increase in the chain length, we have considered the PFBT-T12TT$_n$ and PFBT-T20TT$_n$ oligomers comprising one to five ($n = 1 - 5$) repeating units. We first optimized the ground state structures of the molecules by using DFT calculations with the B3LYP hybrid exchange-correlation functional at the level of 6-31G (d) split valence polarized basis set. This functional uses the non-local correlation provided by the LYP expression, and VWN functional III for local correlation.[41] Fig. 1(b) shows, as an example, the optimized geometry of PFBT-T20TT$_4$. On

the basis of the optimized ground state (S_0) configurations, absorption spectra of the molecules solvated in chlorobenzene were then obtained by using the time-dependent density functional theory (TD-DFT) method at the B3LYP/6-31G(d) level. In calculating the spectra in solutions, the polarized continuum model (PCM) was adopted to model solvent effects. All the quantum chemistry based calculations in this work have been carried out using the Gaussian 09 package.[42]

In order to examine the properties at room temperature, we further adopt an approach combining DFT calculations with MD simulations for a specific case of $n = 4$ for each of the molecules. The initial geometry was subjected to an energy minimization procedure by stepwise use of steepest-descent, conjugate-gradient methods. The optimized structure was then subjected to MD simulations under the NVT ensemble (constant number of moles, volume and temperature) during which temperature is maintained constant at 298 K by the Berendsen thermostat[43] with a decay constant of 0.1 ps. The interatomic forces are derived from the all-atom general purpose Universal Force Field[44] (UFF) and the equations of motion are integrated with a time step of 1 fs. UFF has been employed by a number of studies on organic systems.[45,46] It is worthwhile to note that the appropriate forcefield had been chosen via a judicious comparison of the configuration obtained via DFT-optimization and those obtained via geometry optimization with different classical forcefields. It was found that that the structures of PFBT-T20TT and PFBT-T12TT optimized with COMPASS and PCFF forcefields, the two common forcefields for MD simulations of polymers, deviate much more strongly from the respective DFT-optimized conformations (in terms of dihedral distortions and symmetry of bond-lengths in five-membered rings) as compared to that optimized with UFF. Following the initial 50 ps period during which the system is slowly heated to 300 K, MD simulations are continued yielding the production run trajectory of 1 ns. The geometry optimization and the MD simulations are carried out with the Forcite module available in Materials Studio. We have then extracted the atomic coordinates at an interval of 50 ps, yielding an ensemble of 20 conformations. By subjecting each of these conformations as an input to the DFT calculations at B3LYP/6-31G(d) level for calculation of average energy of the HOMO. As MD simulations are computationally efficient, these combined DFT-MD calculations have been carried out on molecules with the large alkyl substituent groups.

B. The multi-mode Brownian oscillator model

The influence of molecular vibrations on the electronic structure of organic molecules can be studied by employing the multimode Brownian oscillator (MBO) model. In a previous work,[36] we have successfully demonstrated the viability of the MBO model for modeling the absorption and emission spectra of conjugated polymers, in which the electron-phonon coupling is recognized to be an essential consideration. In this model, the electronic degree of freedom is abstracted as a two-level system with the ground state being $|g\rangle$ and one of the most important excited states being $|e\rangle$. The two-level system is coupled to a set of primary oscillators, which are in turn coupled linearly to a bath of secondary phonons. The model Hamiltonian for the MBO model is written as[28]

$$H = |g\rangle H_g \langle g| + |e\rangle H_e \langle e| + H', \tag{1}$$

where

$$H_g = \sum_j \left[\frac{p_j^2}{2m_j} + \frac{1}{2} m_j \omega_j^2 q_j^2 \right], \tag{2}$$

$$H_e = \hbar\omega_{\rm eg}^0 + \sum_j \left[\frac{p_j^2}{2m_j} + \frac{1}{2} m_j \omega_j^2 (q_j + d_j)^2 \right], \tag{3}$$

and

$$H' = \sum_n \left[\frac{P_n^2}{2m_n} + \frac{1}{2} m_n \omega_n^2 \big(Q_n - \sum_j \frac{c_{nj} q_j}{m_n \omega_n^2}\big)^2 \right]. \tag{4}$$

In the equations above, $p_j(P_n)$, $q_j(Q_n)$, $m_j(m_n)$, and $\omega_j(\omega_n)$ represent the momentum, the coordinate, the mass, and the angular frequency of the j-th (n-th) nuclear mode of the primary (secondary) oscillators, respectively; d_j denotes the displacement of the j-th nuclear vibrational mode for the electronic excited state; $\hbar\omega_{\rm eg}^0$ stands for the energy gap (E_{eg}) of the two-level system; and H' describes the secondary phonons which linearly couple to the primary oscillators with the respective strengths c_{nj}.

Based upon the Hamiltonian (1), calculation of the linear absorption spectrum can be carried out in a straightforward manner. We can obtain an expression for the absorption intensity as,[28]

$$I(\omega) = \frac{1}{\pi} \mathrm{Re} \int_0^\infty dt \exp\big(i(\omega - \omega_{\rm eg}^0) + \lambda)t - g(t)\big) \tag{5}$$

where $\lambda = \sum_j \lambda_j$ with λ_j being half of the Stokes shift for the j-th mode. The lineshape function denoted vy $g(t)$, in the equation above is defined as

$$g(t) = \frac{1}{2\pi} \int_{-\infty}^{\infty} d\omega \frac{C''(\omega)}{\omega^2} \big[1 + \coth(\beta\hbar\omega/2)\big] \big[e^{-i\omega t} + i\omega t - 1\big]. \tag{6}$$

where β is the inverse temperature and the function $C''(\omega)$ is the summation of $C_j''(\omega)$ defined with

$$C_j''(\omega) = \frac{2\lambda_j \omega_j^2 \omega \gamma_j}{\omega^2 \gamma_j^2 + (\omega_j^2 - \omega^2)^2}. \tag{7}$$

Important parameters introduced herein include λ_j as the reorganization energy and γ_j as a damping coefficient, the physical significance of which will be discussed in a latter section. For convenience, we employ the Huang-Rhys factor $S_j \equiv \frac{\hbar\omega_j}{\lambda_j}$ to denote the coupling strength between electron and the primary oscillators.

Table I: The calculated average bond length (R) between atoms C2 and C3 and the angular difference between fragment 1 and fragment 2 defined by the dihedral angle (α) for S1-C2-C3-S4 atoms.

	PFBT-T12TT		PFBT-T20TT	
	R	α	R	α
n=1	1.449	152.45	1.456	-134.86
n=2	1.448	157.77	1.455	-134.09
n=3	1.447	159.37	1.455	-135.37
n=4	1.446	162.67	1.455	-135.83
n=5	1.446	160.55	1.455	-136.69

Table II: The calculated energy level of HOMO, LUMO, and energy gap for PFBT-T20TT and PFBT-T12TT. The corresponding experimentally measured[11] HOMO energies are listed for comparison (in eV) along with the band gaps and LUMO energies estimated from UV-spectra which are denoted in brackets.

	PFBT-T20TT			PFBT-T12TT		
	DFT	DFT-MD	Exp	DFT	DFT-MD	Exp
E_{HOMO}	-4.90	-4.96	-5.05	-4.63	-4.98	-5.33
E_{LUMO}	-2.94	-2.98	(-3.46)	-3.05	-3.00	(-3.78)
ΔE_{L-H}	1.96	1.98	(1.59)	1.58	1.98	(1.55)

III. RESULTS AND DISCUSSION

A. Molecular geometry and orbital energy structure

We have first optimized the ground state (S_0) conformations of PFBT-T12TT and PFBT-T20TT molecules with $n = 1 - 5$ at the B3LYP/6-31G (d) level of theory. Important structural parameters of the optimized geometries such as the dihedral angle α (S1-C2-C3-S4) between the thiophene in the 5,6-difluoro-4,7-di(thiophen-2-yl)benzo[c][1,2,5]thiadiazole (fragment 1) and thieno[3,2-b]thiophene (fragment 2) and the average bond length between the C-atoms connecting them are listed in Table I. These average bond lengths are between 1.45 Å and 1.46 Å. Compared with the pendant straight alkyl chain substituted PFBT-T12TT, the branched alkyl chain substituted PFBT-T20TT exhibits a more distorted structure.[40] The absolute values of the dihedral angles between the two fragments are smaller in PFBT-T20TT oligomers. The angle of distortion between two fragments in PFBT-T20TT$_4$ is thus 44.17°, which is larger than the value of 17.33° in PFBT-T12TT$_4$. Such differences in the conformations brought about by the difference in the straight and branched substituting alkyl chains may thus have significant implications in extracting high performance in the photovoltaic devices.

To analyze the characteristics of frontier molecular orbitals obtained via DFT method, we have calculated the energies of the highest occupied molecular orbital $E_{\rm HOMO}$, the lowest unoccupied molecular orbital $E_{\rm LUMO}$, and the energy difference between them $\Delta E_{\rm L-H}(\equiv E_{\rm LUMO} - E_{\rm HOMO})$. Each of these properties is found to exhibit a linear dependence on n^{-1} implying convergence with an increase in n, using which we can calculate extrapolated values for infinitely long polymer chains. Such values for both types of oligomers are listed in Table II under the columns labeled DFT. The corresponding values measured or estimated experimentally[11] are also listed for comparison. While the calculated value of $E_{\rm HOMO}$ agrees well with the experimental data for PFBT-T20TT, that for PFBT-T12TT is deviates from experimental value by nearly 0.7 eV. The calculated values of $E_{\rm LUMO}$ for both materials, on the other hand, are quite different from the experimental data. In consequence, the purely DFT-based calculations yield ΔE_{L-H} which reproduces experimental values well for PFBT-T12TT but not for PFBT-T20TT.

It is well known that the molecular distortions in the organic systems impact both the energy level structures as well as the optical and electronic properties. In order to take into account the structural changes due to molecular vibrations at room temperature (298 K), we examine both the oligomers with $n = 4$ and employ a methodology combining DFT calculations with MD simulations (DFT-MD) as discussed at the end of section II A. The subsequently calculated average values of different properties are listed in Table II under the columns labeled DFT-MD. Interestingly, $E_{\rm HOMO}$ for PFBT-T12TT yielded by this approach is nearly 0.35 eV lower than that obtained via DFT calculations, and in better agreement with the measured value. Similar, albeit marginal, improvement in comparison of experimental $E_{\rm HOMO}$ is achieved for PFBT-T20TT as well. The discrepancy between the calculated and experimental values, especially for PFBT-T12TT, may originate partly from the lack of explicit solvent effects in the calculations or influence of inter-chain interactions in thin-film state, which may lead to entangled conformations of long polymer chains. The values of $E_{\rm LUMO}$ remain relatively similar in the results obtained with both the approaches. Quite importantly, it is found that the average $E_{\rm HOMO}$ and $E_{\rm LUMO}$ from DFT-MD approach are each nearly the same between both the polymers. This finding is likely to be of great significance for assessing device performance, as the open circuit voltage ($V_{\rm oc}$) in the solar cells fabricated with these two materials have been measured to be nearly identical.[11] To emphasize that the conformational sampling in the DFT-MD approach was reliable, we show in Fig.2 the scatter plots of $E_{\rm HOMO}$, $E_{\rm LUMO}$ and the difference between the two in which all the values can be observed to fluctuate about their average values. Furthermore, in the linear response approximation, we assume the same parabolic shape of the potential energy surfaces for the ground and excited states and accordingly, the reorganization energy can be estimated to be 0.201 eV and 0.502 eV for PFBT-

Table III: The vertical excitation energies(E_v), absorption wavelength(λ), the ratio of the oscillator strength to the number of monomer units (f/n) corresponding to different excited states (ES) along with the percentage contributions from transitions between different orbitals as calculated for PFBT − T20TT$_n$ ($n = 1 - 5$) at the TD-B3LYP/6-31G (d) level in chlorobenzene solution.

n	ES	E_v (eV)	λ (nm)	f/n	Transition		Nature
1	1	2.1181	585.37	0.6543	H → L	99%	ICT
	4	3.3095	374.63	0.9135	H → L+1	93%	$\pi \rightarrow \pi^*$
2	1	1.8821	658.76	0.8218	H → L	95%	ICT
	7	2.9426	421.35	0.7196	H → L+2	94%	$\pi \rightarrow \pi^*$
3	1	1.8033	687.55	0.8612	H → L	88%	ICT
					H-1 → L+1	7%	
	13	2.8768	430.98	0.6799	H → L+3	83%	$\pi \rightarrow \pi^*$
					H-1 → L+4	10%	
4	1	1.7757	698.25	0.88916	H → L	78%	ICT
			(700)		H-1 → L+1	13%	
	22	2.8571	433.95	0.6400	H → L+4	68%	$\pi \rightarrow \pi^*$
			(440)		H-1 → L+5	14%	
5	1	1.7636	703.01	0.9191	H → L	68%	ICT
					H-1 → L+1	17%	
	34	2.8504	434.97	0.6533	H → L+5	60%	$\pi \rightarrow \pi^*$
					H-1 → L+6	18%	

T20TT$_n$ and PFBT-T12TT$_n$, respectively.

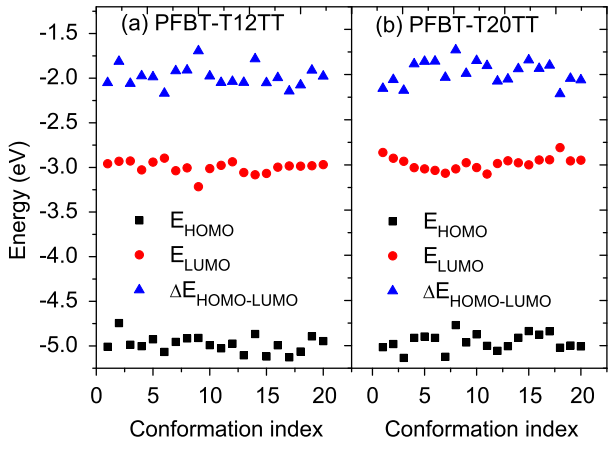

Figure 2: The scatter plots of E_{HOMO}, E_{LUMO} and the difference between the two ($\Delta E_{\mathrm{HOMO-LUMO}}$) for (a) PFBT-T12TT and (b) PFBT-T20TT.

B. Optical properties using quantum chemical calculations

The two materials investigated in this paper are known to be low-band gap polymers, yet, the calculations of $E_{\mathrm{L-H}}$ have yielded a value of nearly 2 eV for both the materials, starkly different from measured values. Considering the relatively well-reproduced E_{HOMO}, this discrepancy partly arises due to the relatively large differences in the values of calculated and measured values of E_{LUMO}. While the experimental value of HOMO energy is measured straightforwardly from oxidative peaks in the cyclic voltammetry measurements, that of LUMO is estimated from the value of the optical band gap rendering it difficult to be compared with theoretical calculations.

In order to characterize the features of the band gap for both the polymers, in the following two subsections, we discuss the optical properties in detail. Firstly, we have carried out TD-DFT calculations on the optimized S_0 structures of PFBT-T20TT$_n$ ($n = 1 - 5$). The vertical excitation energies (E_v), absorption wavelengths (λ), oscillator strengths (f), and the contributions to different excited states by the frontier orbital energy levels are obtained and presented in Table III. PFBT-T20TT exhibits two important absorption bands in chlorobenzene solution and the wavelengths of absorption peaks of both the bands increase with the extension of the oligomeric chain. For PFBT-T20TT$_{4(5)}$, the calculated λ for the two bands are 698 nm (703 nm) and 434 nm (435 nm), which are in excellent agreement with the experimentally measured values of 700 nm and 440 nm shown in parenthesis in Table III. Convergence of the vertical excitation energies and the scaled oscillator strengths with respect to number of monomeric units is readily evident. The PFBT-T20TT$_4$ structure thus provides a good choice of system to predict the optical properties of this polymer by quantum chemical calculations, allowing for a balance between accuracy of results and the computational expense. More importantly, the vertical excitation energy is found to be 1.78 eV for PFBT-T20TT$_4$ and 1.48 eV for PFBT-T12TT$_4$ (not shown here). In contrast to the calculated values presented in Table II, we can observe that the values of energy gap presented here are much closer to those found in experiments. It is thus imperative to examine in further details the molecular orbitals participating in the respective transitions.

To this end, the calculated electronic density distribution plots for the primary participating transition orbitals are depicted in Fig. 3 for PFBT-T20TT$_4$ and PFBT-T20TT$_5$. Firstly, it can be noted that the electron density for all the transition orbitals resides in the backbone chains of the polymer and not on the alkyl side groups. This lends support to the reliability of our calculated results which are obtained by substituting larger alkyl groups with the smaller counterparts for computational efficiency. Secondly, we can find for the PFBT-T20TT$_4$, the HOMO is almost delocalized on the central π-conjugated segments, and the LUMO+4 ex-

hibits the anti-π bonding characteristics. The transition from HOMO to LUMO+4 can then be attributed to $\pi \rightarrow \pi^*$ transition, which dominates the smaller wavelength band. For the long wavelength band in PFBT-T20TT$_4$, the electronic transition corresponds mainly to HOMO $\rightarrow$ LUMO transition that is found to carry characteristics of intramolecular charge transfer (ICT). We note that even though these calculations do not take into account possible localization effects induced by the molecular distortions in the room temperature MD simulations, the conclusions about the nature of excited states remain valid since the molecular distortions do not change the π and π^* features of the orbitals. As a result, the values of vertical energy gap presented in this subsection compare reasonably well with the experimental data and allows to predict the characteristics of HOMO $\rightarrow$ LUMO transition observed in the experiments to be of ICT nature. Calculations on PFBT-T12TT$_4$ have also been carried out (not shown) and they are found to exhibit similar characteristics with respect to localization of electron density and nature of excited states.

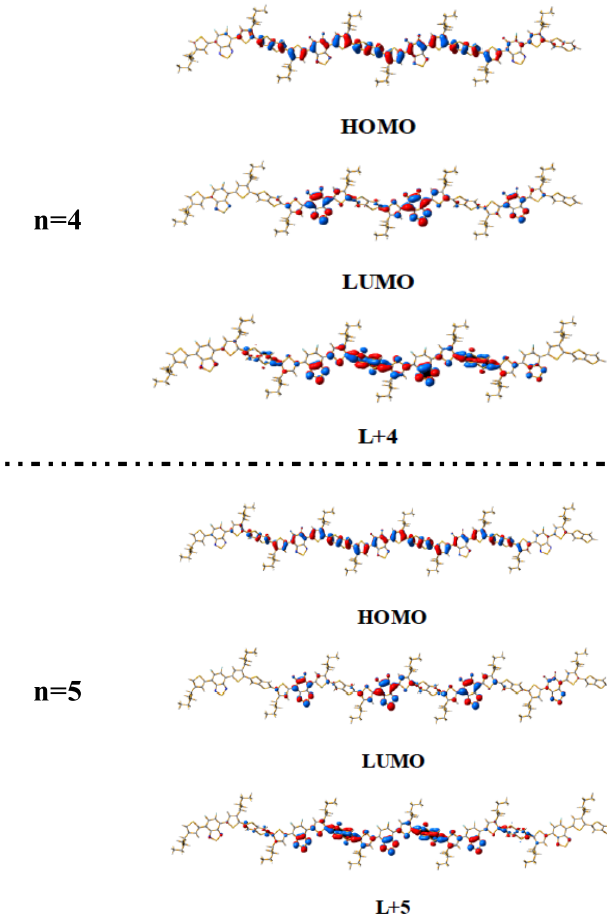

Figure 3: The electronic density plots of HOMO and LUMOs in PFBT $-$ T20TT$_{\rm n}$ ($n = 4 - 5$).

C. Analyzing the absorption spectra using the MBO model

Results presented in the previous subsections indicate the electronic transitions characteristics are similar in PFBT-T12TT and PFBT-T20TT. With the combined DFT-MD approach, we also find that it is important to take into account the molecular distortions via configurations sampling of an MD trajectory to obtain improved results, especially for PFBT-T12TT. Thus, in order to further elucidate the influence of molecular vibrations on the optical properties of these high performance donor materials in PSCs, we have employed the MBO model to calculate their absorption spectra at room temperature. This model is useful to investigate an electronic-two-level system embedded in a phonon environment. The key parameters of the model are the frequencies of the primary oscillators ω_j, the Huang-Rhys factors $S(\equiv \sum_j S_j)$, and the damping coefficients $\gamma(\equiv \sum_j \gamma_j)$; while other parameters include the temperature and the $0 - 0$ transition energy. The frequency of a primary oscillator dominates the energy separation between the zero phonon line (ZPL) and the one-phonon peak while the corresponding Huang-Rhys factor reflects the respective coupling strength. The parameter γ is responsible for the coupling strength of the primary oscillator and the bath modes, thereby determining the broadening of the ZPL and its phonon side bands. The absorption spectra calculated with this model are found to exhibit excellent fitting of the experimental data as shown in Fig. 4 for both PFBT-T12TT and PFBT-T20TT, in chlorobenzene solution as well as in thin-film state at room temperature. All the main features of the experimentally obtained spectra including the shoulder-peaks have been fitted satisfactorily by using a set of parameters enlisted in Table IV. The coupling of the high-frequency modes with the two-level system determines the overall line shape whereas the low-frequency modes provide additional broadening of the peaks. During the fitting procedure, the value of $E_{\rm eg}$ is taken from the corresponding peaks in the absorption spectra measured experimentally. The initial value of ω in the high frequency region is usually taken as the spacing between the highest and the next highest peak. The initial value of γ is determined by the overall line shape of the spectrum, usually taken as one third of corresponding ω.

The absorption spectrum of PFBT-T12TT in thin-film state is found to be red shifted from that in solution, reflecting an enhancement of interchain interactions in the solid state, and thus a higher degree of ordering. The extracted values of Huang-Rhys factors (S_2, S_3) for the high-frequency modes are found to be larger in PFBT-T12TT than in PFBT-T20TT for both solution and solid state, pointing to a higher exciton-phonon coupling strength in the former. Consequently, relatively large reorganization energy is expected for this material, which may be attributed to its linear side chains, which are relatively more flexible than the bulky side chains of PFBT-

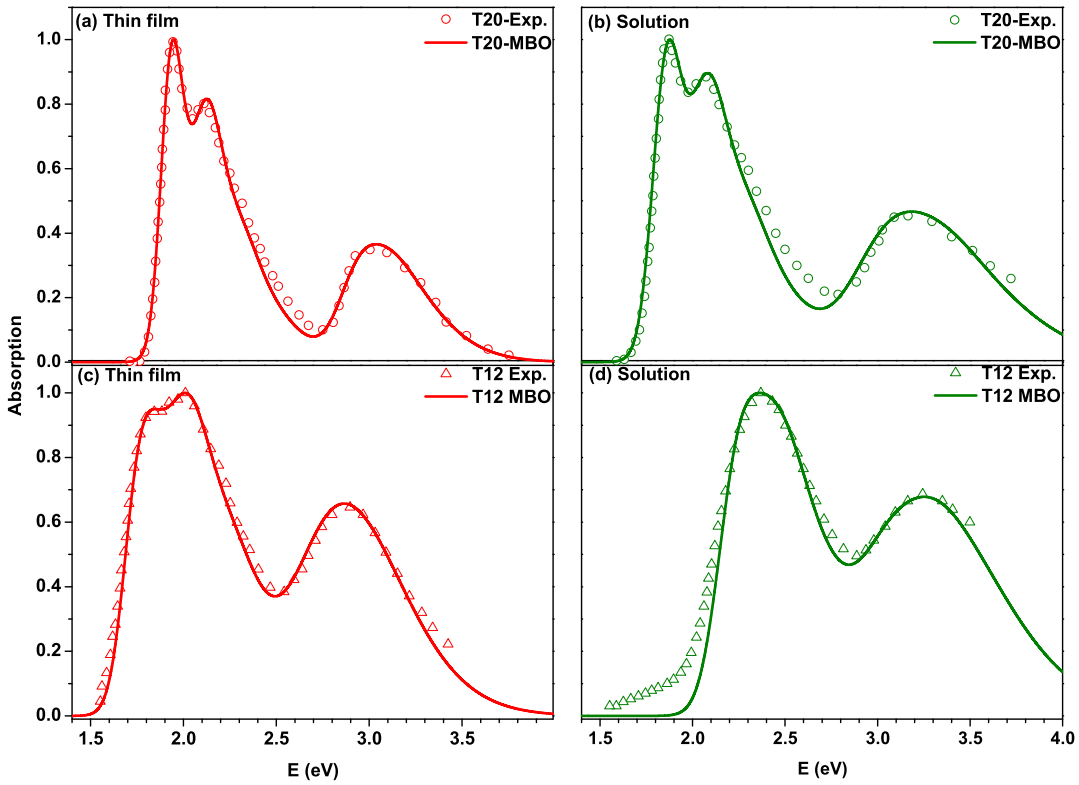

Figure 4: The absorption spectrum calcluated from the MBO model (solid curves) for (a)-(b) PFBT-T20TT and (c)-(d) PFBT-T12TT as fitted to their measured experimental spectra (hollow symbols) in thin-film state (left panels) and in chlorobenzene solution (right panels). All the fitting parameters employed are lilsted in Table IV.

Table IV: Parameters (the frequencies of the primary oscillators ω , the damping coefficients γ, and the Huang-Rhys factors S) of the MBO model employed for fitting the absorption spectra of PFBT-T20TT and PFBT-T12TT in thin film and solution.

In thin film	$\gamma_1(cm^{-1})$	$\gamma_{2/3}(cm^{-1})$	$\omega_1(cm^{-1})$	$\omega_{2/3}(cm^{-1})$	S_1	$S_{2/3}$	E_{eg}(eV)
PFBT-T20TT(1)	200	850 (300)	100	1900 (1400)	4.0	0.66 (0.37)	1.86
PFBT-T20TT(2)[1]	260	250	400	1700	4.7	0.74	2.54
PFBT-T12TT(1)	300	500 (200)	180	2100 (900)	3.8	0.92 (0.75)	1.89
PFBT-T12TT(2)[2]	260	250	500	2100	7.5	0.7	2.34
In solution							
PFBT-T20TT(1)	200	850 (300)	100	1900 (1400)	4.8	0.65 (0.44)	1.85
PFBT-T20TT(2)[3]	260	250	400	2300	8.9	0.74	2.32
PFBT-T12TT(1)	300	500 (200)	180	2100 (900)	8.0	0.80 (0.75)	2.23
PFBT-T12TT(2)[4]	260	250	500	2400	8.0	0.98	2.61

[1] A weighting factor of 0.36 was applied to the spectrum of PFBT-T20TT (2) before being added to PFBT-T20TT (1) to obtain the final spectrum.
[2] A weighting factor of 0.615 was applied to the spectrum of PFBT-T12TT (2) before being added to PFBT-T12TT (1) to obtain the final spectrum.
[3] A weighting factor of 0.46 was applied to the spectrum PFBT-T20TT (2) before being added to PFBT-T20TT (1) to obtain the final spectrum.
[4] A weighting factor of 0.645 was applied to the spectrum PFBT-T12TT (2) before being added to PFBT-T12TT (1) to obtain the final spectrum.

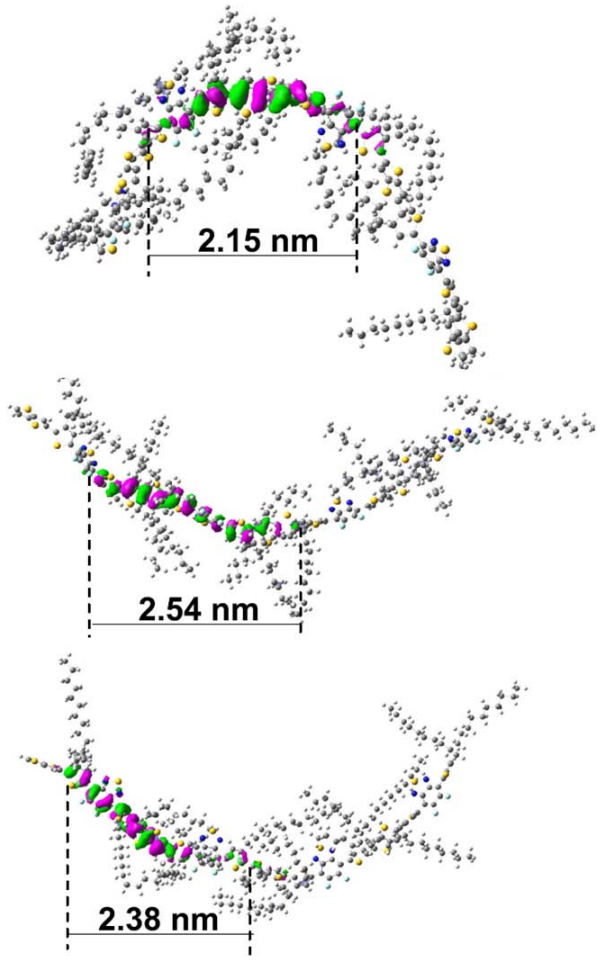

Figure 5: The electronic density distribution plots for the HOMO in three conformations sampled from the MD simulations trajectory of PFBT-T20TT$_4$.

T20TT. Correspondingly, the higher Huang-Rhys factor for PFBT-T12TT in the solid state as compared to that in the solution may imply a decrease in the localization length of the electronic wavefunction. Furthermore, the measured shape of absorption spectrum of PFBT-T20TT in thin film state was found to be nearly identical to that in the solution.[11] In contrast with the trend for PFBT-T12TT, such spectral similarity in PFBT-T20TT is significant as it suggests the ordering of the excited states in PFBT-T20TT to remain unchanged between the thin-film state and the solution state, leading to a better device performance. This similarity was argued to have been originated from the presence of the bulky branched alkyl chain substituted groups that inhibit PFBT-T20TT from attaining any significantly higher degree of ordering in the thin-film state than in solution.

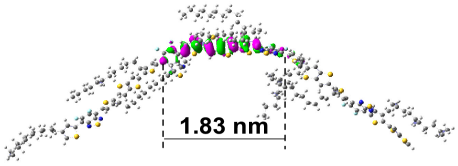

Figure 6: The electronic density distribution plot for the HOMO in one randomly sampled conformation from the MD simulations trajectory of PFBT-T12TT$_4$.

D. Localization of wave functions

In this subsection, we discuss on the implications of the revealed features of the energy level structure on the device performance. It has been observed, in the comparison PSCs based on PFBT-T20TT and PFBT-T12TT,[11] that the open circuit voltages V_{oc} for the two cases are almost identical. The short-circuit current I_{sc} for the device with PFBT-T20TT/PC$_{71}$BM heterojunction is, hoewever, nearly two orders of magnitude larger than that with PFBT-T12TT/PC$_{71}$BM, indicating the greater charge-carrier mobility in the PFBT-T20TT. The nearly identical V_{oc} is well supported by our calculations based on DFT-MD approach, which yield values of HOMO and LUMO energies that are fairly similar in both the oligomers.

Our results further suggest that the conformational distortions such as bending and twisting result in a greater influence on the molecular orbital energy structure for the PFBT-T12TT than PFBT-T20TT. For further insight into such effects, we have calculated the electronic density plots corresponding to the HOMO for sample molecular geometries extracted from the MD simulation trajectories at 298 K. Fig. 5 shows such plots for three randomly sampled conformations of PFBT-T20TT$_4$, and Fig. 6 for one geometry of PFBT-T12TT$_4$. It can be noted that the electron density distributions span nearly two monomeric units in the former and slightly less in the latter. However, compared to similar plots shown in Fig. 3 for ground state optimized geometries, one may expect the electronic wave functions more likely to be spatially localized in the room-temperature samplings owing to the conformational distortions of the oligomer backbone chains. This effect is stronger for PFBT-T12TT$_4$, as the localization length of PFBT-T12TT ($\sim$ 1.8nm) is much smaller than that of PFBT-T20TT ($\sim$ 2.4nm). This difference may point towards a lower intra- and intermolecular charge transfer rates in the former than the latter, which implies a relatively lower mobility, leading consequently to the smaller I_{sc} in the devices based on it.[47] A recent study employed the pump-push-probe technique to elucidate the importance of delocalized CT state in the polymers (PFB, P3HT, MDMOPPV and PCPDTBT) which are usually used in PSCs.[13] In their work, they highlighted that due to the heterojunction configurations with acceptor materials like C60, the delocalization of HOMO (see Fig. 2b

therein Ref.[13]) across the donor polymeric materials acts as gateways for the subsequent charge separation. Following this view-changing proposition, increasingly more understanding of the role of delocalization in donor materials in governing performance of PSCs has emerged. Our work thus employs the identical core idea as the two donor materials we have studied had been used in the original experimental study in conjunction with $PC_{71}BM$ as active layer to fabricate and subsequently characterize heterojunction PSC devices.[11] We thus propose that the greater HOMO delocalization in PFBT-T20TT as compared to PFBT-T12TT facilitates easier formation of charge separated states thereby leading to improved mobility and device performance. Our argument is also in agreement with the most recent study on PFBT-T20TT based devices,[48] wherein it was found that the more efficient hole transport results in PFBT-T20TT intercalated with C60 as compared to pure polymer.

In order to lend more support towards the intuitive picture presented here on the relationship between mobility and the wavefunction localization, we have further ventured to calculate the exciton wavefunction diffusion fully quantum mechanically, by modeling the two polymer materials as infinitely long one-dimensional chains. Details of the methodology employed and key results are described in the Appendix, in order to retain the focus of this paper on the dual approach of quantum-chemistry calculations and the MBO model calculations. From Fig. 7, one can observe that the exciton diffusion is much faster in PFBT-T20TT than in PFBT-T12TT, in qualitative agreement with the properties inferred from the DFT-MD results.

IV. CONCLUSIONS

In summary, we have have carried out theoretical and computational investigation of the optical properties of two novel low band gap polymers PFBT-T20TT and PFBT-T12TT, which exhibit promising applications as donor materials in polymer solar cells. The molecular structures of the two polymers differ from each other only in terms of substituent alkyl groups, yet, such difference leads to significant changes in the electronic properties with the former showing much greater short-circuit current. In this work, we have adopted a dual-faceted theoretical approach to study the molecular properties of materials via combined quantum chemistry and molecular dynamics based calculations as well as calculating their absorption spectrum with the MBO model. Our results demonstrate that the calculated HOMO energy is well in agreement with the experimental measurements in both the materials. Especially for PFBT-T12TT, significant improvement in the calculated values of HOMO energy is obtained with the DFT-MD approach over purely DFT approach, indicating the essential role of molecular vibrations. The straying of calculated energy gap between HOMO and LUMO from the experimental values, has been attributed to the estimations employed in the experiments, which yields the optical band gap, rather than HOMO to LUMO gap. Nevertheless, nearly identical values of the HOMO to LUMO energy gaps are found from the DFT-MD approach in both the molecules, well in agreement with the similar values of V_{OC} measured in the devices based on them. Calculations of the electronic excited states with TD-DFT methods for both the molecules have further helped reveal the nature of electronic transitions to be of intramolecular charge transfer for the low-energy excitations and of $\pi \rightarrow \pi^*$ transition for high-energy excitation. We further employ the MBO model in order to calculate the absorption spectrum of these materials in both the thin-film state as well as in solution state. The MBO model is a well established model for probing the influence of coupling of an electronic two-level system with a primary bath of high frequency phonon modes coupled in turn to a secondary bath. Excellent fitting with the experimentally measured spectra has been obtained and the fitting parameters thereby extracted help generate insights into the properties of these materials. Higher values of Huang-Rhys factors extracted for PFBT-T12TT in comparison to PFBT-T20TT point to the stronger exciton-phonon coupling in the former. This finding finds support through the DFT-MD calculations, which are shown to be important in calculation of more accurate HOMO energy in PFBT-T20TT. The role of conformational distortions in influencing the localization of the electronic wave functions has also been identified.

The performance of polymer solar cells is typically assessed with key characteristics such as short-circuit current, the open-circuit voltage and the fill factor. In the devices based on the the two polymers studied in this work show that the I_{SC} is greatly enhanced in PFBT-T20TT than PFBT-T12TT, yet V_{OC} and the fill factor remain nearly the same. Combined the above two aspects of the present work, we are then able to understand the novel device performance of the two materials. Our results show that as the electrons mainly reside on the backbone of the polymers, the branched versus straight configuration of the side chains does not lead to any appreciable difference in the energetic structure of PFBT-T20TT and PFBT-T12TT. The nearly identical HOMO-LUMO gap of the two molecules found from DFT-MD simulations implies the V_{OC} to also remain relatively similar. Furthermore, the electronic wavefunction is more delocalized on the backbone structure of PFBT-T20TT than PFBT-T12TT due to the molecular distortions. Accordingly, the mobility of electrons and thus the I_{SC} is largely enhanced in the former. Synergetic application of different molecular simulations and theoretical techniques is thus demonstrated to be a viable strategy yielding insightful results on the electronic properties of the semiconducting polymeric materials and the devices based on them. Tracing the origins of disparate electronic properties of two seemingly similar novel low band gap polymers via studying the optical properties, our work is

hoped to open a fresh research outlook.

Acknowledgments

We thank Professor Xiao Hu for providing experimental spectra and for stimulating discussions. One of us (JL) benefitted tremendously from many helpful discussions with Dr Jun Ye. This work is supported by the Singapore National Research Foundation through the Competitive Research Programme (CRP) under Project No. NRF-CRP5-2009-04 is gratefully acknowledged. One of us (YY) is supported in part by the NSF of China via Grant Nos. 91333202, 11134002 and 11104035, and the National Basic Research Program of China (Grant No. 2012CB921401).

Appendix

Transport properties of organic materials are usually studied via modeling of a quasiparticle called polaron, which comprises of an electronic excitation interacting with lattice vibrations. The process of polaron formation is well described by the celebrated Holstein model. In order to show an intuitive picture of the influence of electronic localization in the polymeric materials, we employ the Frenkel-Dirac time-dependent variational method, with the so-called Davydov D1 ansatz to qualitatively investigate the real time dynamics of 1D Holstein polaron. The two polymer systems are modeled as one-dimensional chains of molecules by imposing a periodic boundary condition. We the use the aforementioned method, which has been proved to be applicable in the studies of various organic systems, to calculate the diffusion of the wave functions in the one-dimensional chains. We refer to our earlier work[49,50] for the details and formulation of this well-established method, and list here the most important parameters, including the transfer integral J, the Huang-Rhys factor S, and the characteristic phonon frequency ω_0. While values of J employed here correspond to the typical range of values encountered in organic systems, we have adopted the values of the other two parameters, directly from the quantum chemical calculations and the MBO-derived spectral fitting described in this paper for the two materials.

In Fig. 7, we show the time evolution of the exciton residence probability for each system modeled as a chain of 32 units or 'sites'. The excitonic wave function is initially localized at the center of the chain, and starts to propagate along the two branches in opposite directions, which is analogous to conduction electron with a short lifetime. At the same time, the presence of a component of the exciton wavefunction localized around the initially excited unit can also be noted, which is manifested as the self-trapping effect induced by phonons, implying polaron as a stable excitation that could be regarded as the charge carrier. More importantly, it can be readily noticed by

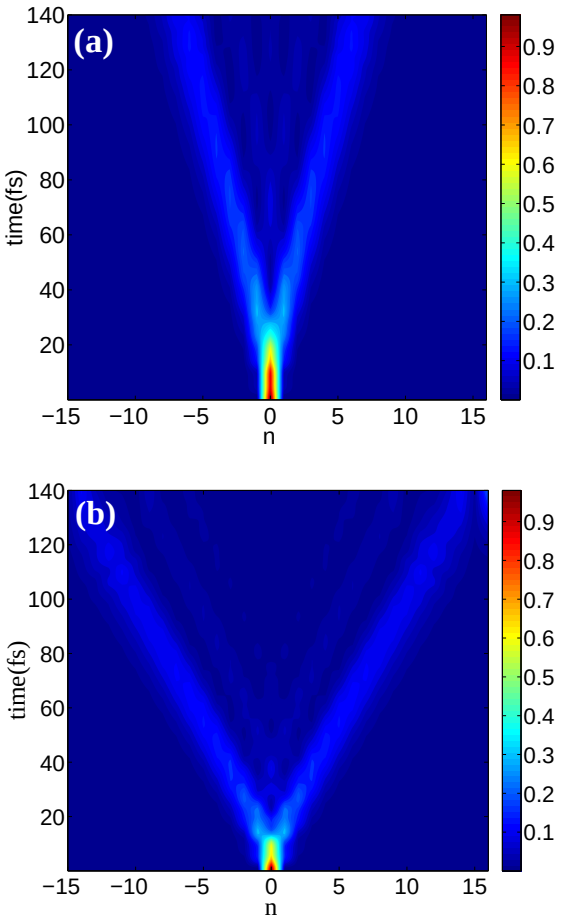

Figure 7: Time evolution of the exciton probability for (a) one dimensional PFBT-T12TT chain with $J = 0.1919, S = 0.92, \omega_0 = 2100\text{cm}^{-1}, \text{W} = 0.8$ and (b) one dimensional PFBT-T20TT chain with $J = 0.3395, S = 0.66, \omega_0 = 1900\text{cm}^{-1}, \text{W} = 0.8$.

comparing Fig. 7 (a) with Fig. 7 (b) that the motion of the exciton is much faster in the model PFBT-T20TT polymer than in PFBT-T12TT. These results are in qualitative agreement with our contention of higher charge-carrier mobility in PFBT-T20TT as compared to PFBT-T12TT resulting from the larger localization length in the former.

[1] S. Günes, H. Neugebauer and N. S. Sariciftci, *Chem. Rev.*, 2007, **107**, 1324-1338.

[2] J. L. Bredas, J. E. Norton, J. Cornil and V. Coropceanu, *Acc. Chem. Res*, 2009, **42**, 1691-1709.

[3] H. Hoppe and N. S. Sariciftci, *J. Mater. Res.*, 2004, **19**, 1924-1945.
[4] T. M. Clarke, J. R. Durrant, *Chem. Rev.*, 2010, **110**, 6736-6767.
[5] G. Yu, J. Gao, J. C. Hummelen, F. Wudl and A. J. Heeger, *Science*, 1995, **270**, 1789-1791.
[6] C. Y. Yang and A. J. Heeger, *Synth. Met.*, 1996, **83**, 85-88.
[7] C. J. Brabec and J. R. Durrant, *MRS Bulletin.*, 2008, **33**, 670-675.
[8] S. C. Price, A. C. Stuart, L. Q. Yang, H. X. Zhou and W. You, *J. Am. Chem. Soc.*, 2011, **133**, 4625-4631.
[9] D. Muhlbacher, M. Koppe, M., P Denk, C. Waldauf, A. J. Heeger, J. Christoph and M. C. S. Brabec, *Adv. Mater.*, 2006, **18**, 789-794.
[10] J. T. Chen and C. S Hsu, *Polym. Chem.*, 2011, **2**, 2707-2722.
[11] Y. Wang, X. Xin, Y. Lu, T. Xiao, X. Xu, N. Zhao, X. Hu, B. S. Ong, and S. C. Ng, *Macromolecules*, 2013, **46**, 9587-9592.
[12] W. Yang, Y. Yao and C. Q. Wu, *Organ. Electron.*, 2013, **14**, 1992-2000.
[13] A. A. Bakulin, A. Rao, V. G. Pavelyev, P. H. M. van Loosdrecht, M. S. Pshenichnikov, D. Niedzialek, J. Cornil, D. Beljonne and R. H. Friend, *Science*, 2012, **335**, 1340-1344.
[14] A. Rao, P. C. Y. Chow, S. Gélinas, C. W. Schlenker, C. Z. Li, H. L. Yip, A. K.-Y. Jen, D. S. Ginger and R. H. Friend, *Nature*, 2013, **500**, 435-439.
[15] S. Gelinas, A. Rao, A. Kumar, S. L. Smith, A. W. Chin, J. Clark, T. S. van der Poll, G. C. Bazan and R. H. Friend, *Science*, 2014, **343**, 512-516.
[16] J. Guo, H. Ohkita, H. Benten and S. Ito, *J. Am. Chem. Soc.*, 2010, **132**, 6154-6164.
[17] S. M. Falke, C. A. Rozzi, D. Brida, M. Maiuri, M. Amato, E. Sommer, A. De Sio, A. Rubio, G. Cerullo, E. Molinari and C. Lienau, *Science*, 2014, **344**, 1001-1005.
[18] V. Coropceanu, J. Cornil, D. A. da Silva Filho, Y. Olivier, R. Silbey and J. L. Bredas, *Chem. Rev.*, 2007, **107**, 926-952.
[19] Z. Shuai, L. Wang and Q. Li, *Adv. Mater.*, 2011, **23**, 1145-1153.
[20] A. Troisi, *Chem. Soc. Rev.*, 2011, **40**, 2347-2358.
[21] E. Hennebicq, G. Pourtois, G. D. Scholes, L. M. Herz, D. M. Russell, C. Silva, S. Setayesh, A. C. Grimsdale, K. Müllen, J. L. Bredas amd D. Beljonne, *J. Am. Chem. Soc.*, 2005, **127**, 4744-4762.
[22] S. Karabunarliev, M. Baumgarten, E. R. Bittner and K. Mullen, *J. Chem. Phys.*, 2000, **113**, 11372-11381.
[23] A. Ferretti, G. Mallia, L. Martin-Samos, G. Bussi, A. Ruini, B. Montanari and N. M. Harrison, *Phys. Rev. B*, 2012, **85**, 235105 1-15.
[24] J. Kleis, B. I. Lundqvist, D. C. Langreth and E. Schröder, *Phys. Rev. B*, 2007, **76**, 1002011-4 .
[25] I. H. Nayyar, E. R. Batista, S. Tretiak, A. Saxena, D. L. Smith and R. L. Martin, *J. Phys. Chem. Lett.*, 2011, **2**(6), 566-571.
[26] T. M. McCormick, C. R. Bridges, E. I. Carrera, P. M. DiCarmine, G. L. Gibson, J. Hollinger, L. M. Kozycz and D. S. Seferos, *Macromolecules*, 2013, **46**(10), 3879-3886.
[27] T. Qin and A. Troisi, *J. Amer. Chem. Soc.*, 2013, **135**, 11247-11256.
[28] S. Mukamel, *Principles of Nonlinear Optical Spectroscopy* Oxford University Press: New York, 1995.
[29] Y. Zhao, V. Chernyak and S. Mukamel, *J. Phys. Chem. A*, 1998, **102**, 6614-6634.
[30] Y. Zhao, R. S. Knox, *J. Phys. Chem. A.*, 2000, **104**, 7751-7761.
[31] J. Ye, Y. Zhao, N. Ng and J. S. Cao, *J. Phys. Chem. B.*, 2009, **113**, 5897-5904.
[32] L. T. Su, A. I. Y. Tok, Y. Zhao, N. Ng, F. Y. C. Boey, J. L. Woodhead and C. J. Summers, *J. Phys. Chem. B.*, 2008, **112**, 10830-10832.
[33] S. L. Shi, G. Q. Li, S. J. Xu, Y. Zhao, and G. H. Chen, *J. Phys. Chem. B*, 2006, **110**, 10475-10832.
[34] S. J. Xu, G. Q. Li, Y. J. Wang, Y. Zhao, G. H. Chen, D. G. Zhao, J. J. Zhu, H. Yang, D. P. Yu, and J. N. Wang, *Appl. Phys. Lett.*, 2006, **88**, 083123 1-3.
[35] R. S. Knox, G. J. Small and S. Mukamel, *Chem. Phys.*, 2002, **281**, 1-10.
[36] J. Ye, A. C. Grimsdale and Y. Zhao, *J. Phys. Chem. A*, 2010, **114**, 504-508.
[37] S. Kilina, E. R. Batista, P. Yang, S. Tretiak, A. Saxena, R. L. Martin and D. L. Smith, *ACS Nano.*, 2008, **2**, 1381-1388.
[38] S. Karabunarliev, E. R. Bittner and M. Baumgarten, *J. Chem. Phys.*, 2001, **114**, 5863-5870.
[39] S. Tretiak, A. Saxena, R. L. Martin and A. R. Bishop, *Phys. Rev. Lett.*, 2002, **89**, 097402 1-4.
[40] T. Liu and A. Troisi, *J. Phys. Chem. C*, 2011, **115**, 2406-2415.
[41] A. D. Becke, *J. Chem. Phys.*, 1993, **98**, 5648-5652.
[42] M. J. Frisch, H. B. Schlegel, G. E. Scuseria, M. A. Robb, J. R. Cheeseman, G. Scalmani, V. Barone, B. Mennucci, G. A. Petersson and H. Nakatsuji, *et al.* Gaussian, Inc., Wallingford CT, 2009.
[43] H. J. C. Berendsen, J. P. M. Postma, W. F. van Gunsteren, A. DiNola and J. R. Haak, *J. Chem. Phys.*, 1994, **81**, 3684-3690.
[44] A. K. Rappe, C. J. Casewit, K. S. Colwell, W. A. Goddard and W. M. Skiff, *J. Am. Chem. Soc.*, 1992, **114**, 10024-10035.
[45] C. D. Wood, B. Tan, A. Trewin, F. Su, M. J. Rosseinsky, D. Bradshaw, Y. Sun, L. Zhou and A. I. Cooper, *Adv. Mater.*, 2008, *20*, 1916-1921.
[46] Z. Chen, E. M. Grumstrup, A. T. Gilligan, J. M. Papanikolas and K. S Schanze, *J. Phys. Chem. B*, 2014, **118**(1), 372-378.
[47] Y. Yao, W. Si, X. Y. Hou and C. Q. Wu, *J. Chem. Phys.*, 2012, **136**, 234106 1-7.
[48] T. Xiao, X. Xu, G. Grancini, J. Q. Mai, A. Petrozza, U.-S. Jeng, Y. Wang, X. Xin, Y. Lu, N. S. Choon, H. Xiao, B. S. Ong, X. H. Lu and N. Zhao, *Sci. Rep.*, 2015, **4**, 5211
[49] B. Luo, J. Ye, C. B. Guan and Y. Zhao, *Phys. Chem. Chem. Phys.*, 2010, **12**, 15073-15084.
[50] J. Sun, B. Luo, and Y. Zhao, *Phys. Rev. B.*, 2010, **82**, 014305 1-14.

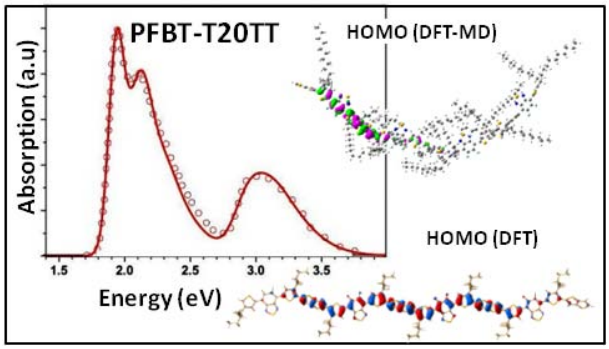

Table of Contents Graphic: Quantum chemistry calculations in combination with MD simulations reveal the influence of alkyl side groups on electronic and optical properties of polymers.